HHS Public Access

Author manuscript

ACS Mater Lett. Author manuscript; available in PMC 2021 October 26.

Published in final edited form as:

ACS Mater Lett. 2020 November 02; 2(11): 1475–1483. doi:10.1021/acsmaterialslett.0c00428.

Photothermal Intracellular Delivery Using Gold Nanodisk Arrays

Chuanzhen Zhao[1,2], **Tianxing Man**[3], **Xiaobin Xu**[1,2,4], **Qing Yang**[1,2], **Wenfei Liu**[1,2], **Steven J. Jonas**[2,5], **Michael A. Teitell**[2,6,7], **Pei-Yu Chiou**[3,6], **Paul S. Weiss**[1,2,6,8]

[1]Department of Chemistry and Biochemistry, University of California, Los Angeles, Los Angeles, California 90095, United States

[2]California NanoSystems Institute, University of California, Los Angeles, Los Angeles, California 90095, United States

[3]Department of Mechanical and Aerospace Engineering, University of California, Los Angeles, Los Angeles, California 90095, United States

[4]School of Materials Science and Engineering, Tongji University, Shanghai 201804, China

[5]Department of Pediatrics, David Geffen School of Medicine, Eli & Edythe Broad Center of Regenerative Medicine and Stem Cell Research, Children's Discovery and Innovation Institute, University of California, Los Angeles, Los Angeles, California 90095, United States

[6]Department of Bioengineering, University of California, Los Angeles, Los Angeles, California 90095, United States

[7]Department of Pathology and Laboratory Medicine, Jonsson Comprehensive Cancer Center, Eli & Edythe Broad Center of Regenerative Medicine and Stem Cell Research, and Molecular Biology Institute, University of California, Los Angeles, California 90095, United States

[8]Department of Materials Science and Engineering, University of California, Los Angeles, Los Angeles, California 90095, United States

Abstract

Local heating using pulsed laser-induced photothermal effects on plasmonic nanostructured substrates can be used for intracellular delivery applications. However, the fabrication of plasmonic nanostructured interfaces is hampered by complex nanomanufacturing schemes. Here, we demonstrate the fabrication of large-area plasmonic gold (Au) nanodisk arrays that enable photothermal intracellular delivery of biomolecular cargo at high efficiency. The Au nanodisks

Corresponding Authors pychiou@gmail.com, and psw@cnsi.ucla.edu.

Author Contributions

The experiments were designed by CZ, TM, PYC, and PSW. Device fabrication was done by CZ, XX, QY, and WL. Delivery experiment was designed and conducted by TM, CZ, and analyzed by TM. Figures were prepared by CZ, TM, and XX. The manuscript was written by CZ, TM, PYC, and PSW with assistance from all other authors. All authors have given approval to the final version of the manuscript.

ASSOCIATED CONTENT

Supporting Information.

Experimental details; Characterization of chemical patterns and stamps; HeLa cell seeding and culturing; Cell fixation; Laser-scanning and delivery setup; Fluorescence microscopy; Cell counting; Numerical simulations; Figure S1: Optical microscope image of cells on 350-nm Au nanodisk arrays; Figure S2: Simulation results for tip temperature on different dimensions of Au nanodisk arrays with laser radiation of 11 mJ/cm^2; Figure S3: Schematic diagram of the optical setup; Figure S4. Delivery efficiency and cell viability results of 0.6 kDa calcein AM using 1-μm wide gold (Au) nanodisk array chips after five runs under 11 mJ/cm^2 laser fluence.

(350 nm in diameter) were fabricated using chemical lift-off lithography (CLL). Nanosecond laser pulses were used to excite the plasmonic nanostructures, thereby generating transient pores at the outer membranes of targeted cells that enable the delivery of biomolecules *via* diffusion. Delivery efficiencies of >98% were achieved using the cell impermeable dye calcein (0.6 kDa) as a model payload, while maintaining cell viabilities at >98%. The highly efficient intracellular delivery approach demonstrated in this work will facilitate translational studies targeting molecular screening and drug testing that bridge laboratory and clinical investigations.

Graphical Abstract

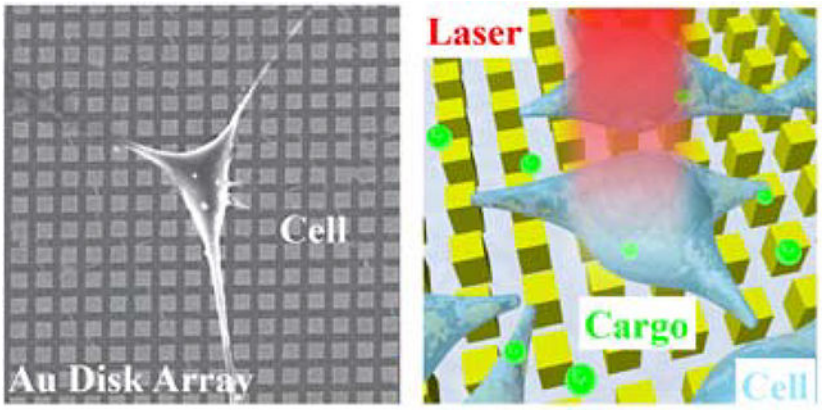

Intracellular delivery of exogenous cargo, such as nucleic acids,[1–4] proteins,[5,6] and membrane-impermeable drugs,[6–8] is of great importance across a spectrum of biomedical and therapeutic applications, including precision gene modification,[9–12] immunotherapy,[13–15] intracellular imaging/sensing,[16,17] drug delivery,[6,8,18,19] and regenerative medicine.[20,21] To date, efforts towards intracellular delivery have been advanced by carrier-based and membrane-disruption-based approaches.[22–24] Viral-vector-based methods remain the most clinically advanced carrier-based strategies, achieving nucleic acid delivery with high efficiencies and specificities.[25,26] However, challenges associated with their potential immunogenicity, safety concerns from off-target effects, complexity, and high costs have limited their broader application.[25] Moreover, viral-based carrier systems suffer from intrinsic limitations in their cargo-carrying capacity, which preclude effective complex biomolecules or mixtures of components. Membrane-disruption-based approaches,[23,27,28] where transient pores are created in cell membranes *via* mechanical,[24,29–35] electrical,[36,37] or photothermal methods,[38–44] are less dependent on cargo and cell type.[45] Electroporation-based methods yield appropriate efficiencies but suffer from low viability and require specialized equipment and reagents.[22,46–49] Strategies using nanostructures, such as nanowires,[50,51] nanostraws,[52–54] and nanoneedles[30,55–58] to create pores in cell membranes, have also been shown to have suitable efficiencies and viabilities for intracellular delivery, but are limited by poor reproducibility, slow processing throughputs, and complicated fabrication processes.

Photothermal strategies that utilize the generation of cavitation bubbles induced by laser irradiation of noble metal nanoparticles or metal plasmonic structures represent another

promising membrane-disruption method.[59,60] Upon laser irradiation, metallic nanostructures absorb incident photon energy through electron oscillations, which results in an abrupt temperature increase in the surrounding aqueous medium.[61,62] Explosive cavitation bubbles nucleate when the temperature exceeds the critical temperature of the aqueous medium.[43] Large fluid shear stress induced by the rapid expansion and collapse of cavitation generates transient and localized pores an adjacent cell membrane.[63] The size of cavitation bubbles dependents on the laser fluences radiated, which has been previously studied to be in the range of 100 nm to 1 μm.[64] Previous studies have demonstrated that noble metal nanoparticles, such as Au nanoparticles, are well suited to serve as high-efficiency delivery agents.[38–44,65,66] However, the cytotoxicity of Au nanoparticles is still under investigation, and this method also suffers from limitations in reproducibility. For example, it has been shown that the number and the location of pores created on each cell is not well controlled due to the random distribution of nanoparticles. Moreover, high delivery efficiencies achieved with increased nanoparticle concentration typically resulted in compromised cell viability.[67] Alternatively, substrate-supported plasmonic structures, fabricated using micro- and nanolithography techniques, serve as promising platforms for high-efficiency and high-viability intracellular delivery.[6,8,19,68] In addition, because of the physical separation of the nanostructures, the stoichiometry of the interactions with the cells can be controlled precisely (as compared to the case for plasmonic nanoparticles). Current methods of producing plasmonic architectures for photothermal delivery applications are limited by time consuming and costly conventional nanolithographic fabrication processes (*e.g.*, electron-beam lithography) used to pattern metal layers, which hinder the scalability of these techniques and represent a critical barrier to applying these technologies to clinical targets. Alternatively, nanofabrication approaches that yield repeatable, scalable, and economical processing of plasmonic nanostructures could facilitate consideration of this approach for wide-scale clinical applications. Recent advances have been made in producing plasmonic structures using template-stripping processes. For example, nanopyramid structures have been fabricated in an economical and high-throughput manner.[8] However, challenges remain for a facile fabrication process as the template stripping process requires the fabrication on a polymer layer and an extra transfer process.

Soft lithography uses soft polymeric stamps to fabricate a range of micro- and nanoscale features in a high-throughput, large-scale, and cost-effective manner.[69,70] Microcontact printing (μCP), as a representative soft lithography method, transfers molecular inks, such as alkanethiols, from stamp to target surfaces.[70,71] A complementary, subtractive soft lithography process chemical lift-off lithography (CLL), uses oxygen plasma-activated polydimethylsiloxane (PDMS) stamps to remove self-assembled monolayer (SAM) molecules selectively from contacted areas on surfaces to create patterns over large areas, and may be used to achieve high-fidelity chemical patterns with line widths approaching 5 nm (corresponding to patterns ~10 molecules across).[72–79] The remaining SAM molecules in the non-lifted-off regions can act as resists to enable selective etching of exposed Au to produce Au nanostructures, such as Au nanolines, nanocircles, and nanosquares.[74,79–81]

In this work, we apply CLL to achieve fabrication of Au plasmonic nanostructures over large areas for photothermal intracellular delivery. Large-area two-dimensional (2D) Au nanodisk arrays are fabricated across centimeter length scales on a variety of substrates,

such as silicon wafers, glass slices, and plastic petri dishes, which provides a significant advantage for versatile intracellular delivery environments and creates opportunities for integration with medical devices. Nanodisk arrays of different sizes have been fabricated in this study to measure delivery efficiencies and cell viabilities as a function of nanostructure surface density per cell. Upon excitation of the nanodisks with a nanosecond laser, delivery efficiencies of >98% and cell viabilities of >98% were achieved using 0.6 kDa cell membrane-impermeable calcein as a model cargo molecule, which is comparable with current photothermal intracellular delivery platforms. This work demonstrates a promising economical and reproducible intracellular delivery approach, with widespread applicability for drug delivery, nanoparticle delivery, and regenerative medicine.

We exploit the plasmonic properties of the gold nanodisks whereby exposure to nanosecond laser pulses generates cavitation bubbles with energies sufficient to puncture cellular membranes, forming pores that facilitate intracellular delivery of desired cargo (Figure 1). HeLa cells, used as a model cell line, were cultured onto CLL-patterned nanodisk substrates and placed in a growth medium containing calcein. By scanning the laser across the wafer-scale Au plasmonic substrate, plasmonic hotspots formed upon illumination. Cavitation bubbles generated at these local regions in contacting the plasma membranes of the target HeLa cells serve as projectiles that render the cells transiently permeable. Cargo molecules within the surrounding medium are able to enter the cytoplasm *via* diffusion.[6] Precision control of the pulsed-laser spot position across the substrate is maintained with a pair of X-Y scanning mirrors. It takes 10 s to scan across the entire 25-mm^2 chip, with over 10^4 cells per chip.

The fabrication of periodic metal nanostructures with micron-scale features can be achieved readily *via* conventional photolithography, while producing sub-micron features often requires specialized tools such as electron beam lithography (EBL) and focused ion beam lithography (FIB). However, these serial writing processes systems are time consuming and costly to operate, leading to extremely limited production yields and output. Transfer printing techniques, such as nanotransfer printing, provide an alternative solution for nanofabrication over large areas while achieving higher processing throughputs.[82] Existing nanoscale printing approaches are limited to certain substrates based on surface energy constraints that are critical for successful and reproducible pattern transfer. In this study, we extend the applications of CLL for biomedical applications. Double-patterning CLL has been recently reported as a means of fabricating Au plasmonic nanodisk arrays (Figure 2a).[81] Polydimethylsiloxane stamps, textured with lines of different widths and pitches are activated by exposure to oxygen plasma to generate hydrophilic silanol groups at the stamp surface. Substrates for CLL (*e.g.*, silicon wafers) are coated with a thin layer of Au (30 nm) that is functionalized with a hydroxyl-terminated alkanethiol (11-mercapto-1-undecanol) SAM. Conformal contact between the stamp and the substrate leads to condensation reactions between OH-groups of SAM and the silanol groups of activated PDMS, leading to the formation of covalent bonds (Si–O–SAM). Lifting the stamp from the substrate results in selective removal of the SAM corresponding to the stamp's pattern, leaving SAM molecules within the non-contacted regions that establish a series of nanoscale lines. A second CLL step was then carried out using a re-activated stamp that is rotated 90° and registered to the initial pattern. After the second patterning step, arrays comprised of SAM nanosquares are

produced, which serve as molecular resists during the subsequent wet etching to generate 2D Au nanodisk substrates.

A representative image of a Au nanodisk array on a petri dish is shown in Figure 2b, where the central area contains uniformly patterned plasmonic nanostructures over cm scales. We extend the capabilities of this technique by demonstrating fabrication on multiple materials (*e.g.*, plastic petri dishes) that are easily coated with Au thin films and then modified *via* CLL patterning (Figure 2c). The ease of integration with commercially available cell culture products demonstrates the potential of our platform to add new functionality to existing medical devices, enabling opportunities for controlled *in situ* drug delivery and molecular screening. Stamps with periodic lines of different feature sizes were used in this study, with widths ranging from 350 nm to 10 μm and pitches ranging from 700 nm to 20 μm. To create sub-micron features, we used commercial optical storage products, such as DVDs (~ $1 each), as masters that contain large-area, periodic gratings with 350 nm wide at 700 nm pitch to circumvent the need for expensive and slow lithographic techniques such as EBL. Atomic force microscope (AFM) images show the morphology of the fabricated Au nanodisks, with widths of 350 nm (Figure 2d), 1 μm (Figure 2e), and 2 μm (Figure 2f). The nanostructures maintain uniform shape with sharp edges, as seen in the AFM images. Corresponding optical microscope images that demonstrate the capability to tune the microscale widths of the patterned structures at 350 nm (Figure S1), 1 μm (Figure 2g), 2 μm (Figure 2h), and 10 μm (Figure 2i).

Plasmonic nanodisk arrays fabricated in this manner are promising candidates for substrates for surface plasmonic resonance (SPR) measurements.[81] Surface plasmon resonance properties of Au nanodisks are studied in separate work.[81] Therefore, we hypothesized that these plasmonic structures could be applied for photothermal delivery, where sharp edges concentrate effectively laser energy to generate cavitation bubbles in the cell culture medium.[68] Explosive boiling of water will occur when the temperature reaches 80–90% of its critical temperature (~650 K) that enables the bubbles formed in close proximity to a cell to puncture its outer membrane discretely.[6,8] Finite element analysis simulations (COMSOL, Multiphysics 4.4) were conducted that estimate that the aqueous cell culture medium reaches above 640 K (~360 °C) locally at laser irradiances of 11 mJ/cm^2 (Figure 3h,i), which is sufficient to initiate cavitation bubble formation. We have performed the simulations on different dimensions of Au nanodisk arrays, which show temperature increases between 636 and 644 K upon laser radiation across different nanodisk array sizes (Figure S2). Calcein AM (AM = acetoxymethyl), a cell membrane permeable variant of calcein, was used for short-term labeling of HeLa cells, as shown in Figure 3a, prior to fixation on a 1-μm wide nanodisk array. A scanning electron microscope (SEM) image of same region after cell fixation (Figure 3b) illustrates that cells are able to adhere to the Au nanodisk arrays substrates. An overlay of the optical and SEM images, within the green box (Figure 3b), is presented in Figure 3c with matching cell distribution and morphology. Results of florescence image of calcein, cell fixation, and an image overlay on 2-μm wide nanodisk arrays are shown in Figure 3d–3f, respectively. Single cell morphology on a 2-μm wide nanodisk array was shown in Figure 3g with diameters of *ca.* 20 μm.

We next demonstrated delivery of Calcein green (0.6 kDa membrane impermeable cargo) with high efficiency and high viability. A schematic of optical setup is shown in Figure S3. Calcein delivery using Au nanodisks (1 μm radius, 2 μm pitch, 30 nm thick) under 11 mJ/cm^2 laser irradiation can be seen in Figure 4a. Hoechst 33342, a cell-permeable nucleus fluorescence dye that emits at 497 nm, was used to label cell nuclei to quantify the total number of cells (Figure 4b). Propidium iodide (PI), which is not permeable to live cells, was used to detect dead cells (Figure 4c). Overlaid images of Calcein green fluorescence, Hoechst 33342 nucleus staining, and PI staining were taken 90 min after laser pulsing and are shown in Figure 4d. Efficiency was determined to be 98 ± 1%, with a viability of 99 ± 1% under the condition described above, with three independent experiments of ~740 cells in total. Control experiments were performed on uniformly flat gold films (30 nm thick) under the same conditions show negligible delivery efficiency, which verifies the critical role of the Au nanostructure in the intracellular delivery of Calcein green under laser irradiation. It has been shown previously for similar systems that the cells will have minimal Au residue after laser radiation.[8]

Different laser fluences, ranging from 7 to 21 mJ/cm^2, were studied to optimize delivery performance (Figure 5a,b). We observed that the number of cells receiving the calcein cargo (green) decreased while cytotoxicity (red) increased with increasing laser fluence. Additional experiments studying the effect of different laser fluences were performed with results plotted in Figure 5e. Over 2,500 cells were counted for each sample tested. Delivery efficiencies increased when the laser fluence was increased from the minimum laser intensity up to 11 mJ/cm^2, reaching 98 ± 1% efficiency. At higher laser fluences, both cell viability and efficiency decreased significantly (with viability decreasing to 16 ± 2% and 6 ± 1% efficiency at 21 mJ/cm^2). We attribute this cytotoxicity to irrecoverable membrane disruption occurring at the higher laser intensities.[6,8,19,83] The delivery efficiency decrease with cell viability is expected, as calcein will only remain in live cells with intact plasma membranes.

We also studied the effects of width and pitch of the periodic nanodisk arrays on delivery performance. Fewer calcein-delivered cells were observed as the sizes of Au nanodisks were increased from 2 μm to 10 μm (Figure 5c,d) while the numbers of dead cells (red) remained the same relative to the total number of cells (blue). This phenomenon can be explained by the density of cavitation bubbles induced by the gold plasmonic structures per cell.[6] Results from our simulations of photothermal response (Figure 3f) indicate that hotspots occur at the corner of each nanodisk where the pitch of nanodisk array is twice the width of an individual disk. Disk arrays with larger disk widths have fewer hotspots and thus form fewer cavitation bubbles. Delivery efficiency therefore decreases on these substrates, due to the smaller numbers of cavitation bubbles. Our data indicate that the delivery efficiency is maximized for disks with widths smaller than 2 μm. Delivery efficiency and cell viability results on nanodisk arrays with different feature widths are shown in Figure 5f. Cargoes with different sizes were also studied, including 0.6 kDa calcein, 4 kDa calcein, and a 150 kDa dextran (Figure 5g). Delivery efficiencies of 98 ± 1% and 94 ± 1% were achieved for 0.6 kDa and 4 kDa calcein, respectively. Decreased efficiency of 36 ± 5% was observed for the dextran, which we infer is related to its lower diffusion coefficient. Note that the gold

nanodisk substrates have the added benefit of being reusable as we did not notice any drop in performance after five experiments (Figure S4).

In summary, effective and safe delivery of biomolecular cargos intracellularly was achieved by exposing large-area gold plasmonic substrates fabricated using double-patterning CLL to nanosecond-laser pulses. Gold surfaces patterned with 2D SAM nanosquare arrays were used to create sub-micron nanostructures. Illuminating the gold nanostructures with nanosecond laser pulses induced cavitation bubbles at the plasmonic hotspots through a photothermal effect. Cells seeded on the nanostructures were rendered transiently porous upon contact with the bubbles, enabling delivery of exogenous biomolecular cargo. Laser fluences and nanodisk sizes were optimized to achieve delivery efficiencies of over 98% for 0.6 kDa calcein with cell viability maintained at over 98%. Note that we attribute the photothermal delivery predominantly to the sheer force generated by the formation and collapse of the cavitation bubble, but we do not exclude the effects of local thermal heating of the plasma membrane.

Desirable features of this CLL-based strategy include: (1) cost-effective and high-throughput fabrication of uniform nanostructures over large (square centimeter) areas, (2) versatile substrate selection, (3) scalability and reproducibility, and (4) economical setup that does not require specialized instrumentation. Efficient delivery of membrane impermeant small molecules to HeLa cells with minimal cell death was achieved, which opens new opportunities for testing and manipulating in disease-relevant cellular targets and potential integration with medical devices. Both the PDMS stamps and the fabricated plasmonic substrates are reusable, enabling scale-up to larger formats. Compared with femtosecond lasers sometimes used in laboratory studies, the nanosecond pulsed laser used here is economical and straightforward to operate. This study demonstrates a promising method for high-efficiency intracellular delivery for cellular therapeutic and drug-discovery applications. In this work, we focused on delivery of small molecules into HeLa cells. Previously, we have shown that our photothermal delivery platform can be applied to deliver large functional cargoes, such as live bacteria, proteins, and plasmids, into a variety of cell types, including primary normal human dermal fibroblasts and human B lymphocyte cells.[22,68] Future optimization and investigations of the Au nanodisk arrays will focus on advancing this technique so as to enable clinical applications, such as gene therapy and cancer immunotherapy.

Supplementary Material

Refer to Web version on PubMed Central for supplementary material.

ACKNOWLEDGMENTS

We gratefully acknowledge support from the National Science Foundation (CMMI-1636136) and the National Institute on Drug Abuse (DA045550). S.J.J. is supported through a NIH Director's Early Independence Award co-funded by the Office of the Director and the National Institute of Dental and Craniofacial Research through the NIH Common Fund, award number DP5OD028181. S.J.J. also wishes to acknowledge Young Investigator Award funds from the Alex's Lemonade Stand Foundation for Childhood Cancer Research, the Hyundai Hope on Wheels Foundation for Pediatric Cancer Research, and the Tower Cancer Research Foundation. P.S.W. and S.J.J. also acknowledge support from the St. Baldrick's Foundation (SBF586729). The authors thank Drs. John M. Abendroth and Jeffrey Schwartz for assistance of writing and useful suggestions. We also acknowledge the facilities

and thank the staff of the Electron Imaging Center, Integrated Systems Nanofabrication Cleanroom of the California NanoSystems Institute.

REFERENCES

(1). Esteban-Fernández de Ávila B; Angell C; Soto F; Lopez-Ramirez MA; Báez DF; Xie S; Wang J; Chen Y Acoustically Propelled Nanomotors for Intracellular siRNA Delivery. ACS Nano 2016, 10, 4997–5005. [PubMed: 27022755]

(2). Ding X; Stewart M; Sharei A; Weaver JC; Langer RS; Jensen KF High-Throughput Nuclear Delivery and Rapid Expression of DNA via Mechanical and Electrical Cell-Membrane Disruption. Nat. Biomed. Eng. 2017, 1, 0039. [PubMed: 28932622]

(3). Xu X; Hou S; Wattanatorn N; Wang F; Yang Q; Zhao C; Yu X; Tseng HR; Jonas SJ; Weiss PS Precision-Guided Nanospears for Targeted and High-Throughput Intracellular Gene Delivery. ACS Nano 2018, 12, 4503–4511. [PubMed: 29536729]

(4). Ball RL; Hajj KA; Vizelman J; Bajaj P; Whitehead KA Lipid Nanoparticle Formulations for Enhanced Co-Delivery of siRNA and mRNA. Nano Lett. 2018, 18, 3814–3822. [PubMed: 29694050]

(5). Yan M; Du J; Gu Z; Liang M; Hu Y; Zhang W; Priceman S; Wu L; Zhou ZH; Liu Z; Segura T; Tang Y; Lu Y A Novel Intracellular Protein Delivery Platform Based on Single-Protein Nanocapsules. Nat. Nanotechnol. 2010, 5, 48–53. [PubMed: 19935648]

(6). Wu YC; Wu TH; Clemens DL; Lee BY; Wen X; Horwitz MA; Teitell MA; Chiou PY Massively Parallel Delivery of Large Cargo into Mammalian Cells with Light Pulses. Nat. Methods 2015, 12, 439–444. [PubMed: 25849636]

(7). Chou LY; Ming K; Chan WC Strategies for the Intracellular Delivery of Nanoparticles. Chem. Soc. Rev. 2011, 40, 233–245. [PubMed: 20886124]

(8). Saklayen N; Huber M; Madrid M; Nuzzo V; Vulis DI; Shen W; Nelson J; McClelland AA; Heisterkamp A; Mazur E Intracellular Delivery Using Nanosecond-Laser Excitation of Large-Area Plasmonic Substrates. ACS Nano 2017, 11, 3671–3680. [PubMed: 28291329]

(9). Yin H; Kanasty RL; Eltoukhy AA; Vegas AJ; Dorkin JR; Anderson DG Non-Viral Vectors for Gene-Based Therapy. Nat. Rev. Genet. 2014, 15, 541–555. [PubMed: 25022906]

(10). Wang HX; Li M; Lee CM; Chakraborty S; Kim HW; Bao G; Leong KW CRISPR/Cas9-Based Genome Editing for Disease Modeling and Therapy: Challenges and Opportunities for Nonviral Delivery. Chem. Rev. 2017, 117, 9874–9906. [PubMed: 28640612]

(11). Zhu H; Zhang L; Tong S; Lee CM; Deshmukh H; Bao G Spatial Control of in vivo CRISPR-Cas9 Genome Editing *via* Nanomagnets. Nat. Biomed. Eng 2019, 3, 126–136. [PubMed: 30944431]

(12). Fang J; Hsueh YY; Soto J; Sun W; Wang J; Gu Z; Khademhosseini A; Li S Engineering Biomaterials with Micro/Nanotechnologies for Cell Reprogramming. ACS Nano 2020, 14, 1296–1318. [PubMed: 32011856]

(13). Qin X-F; An DS; Chen ISY; Baltimore D Inhibiting HIV-1 Infection in Human T Cells by Lentiviral-Mediated Delivery of Small Interfering RNA against CCR5. Proc. Natl. Acad. Sci. U. S. A. 2003, 100, 183–188. [PubMed: 12518064]

(14). Tebas P; Stein D; Tang WW; Frank I; Wang SQ; Lee G; Spratt SK; Surosky RT; Giedlin MA; Nichol G; Holmes MC; Gregory PD; Ando DG; Kalos M; Collman RG; Binder-Scholl G; Plesa G; Hwang WT; Levine BL; June CH Gene Editing of CCR5 in Autologous CD4 T Cells of Persons Infected with HIV. N. Engl. J. Med. 2014, 370, 901–910. [PubMed: 24597865]

(15). Rosenberg SA; Restifo NP Adoptive Cell Transfer as Personalized Immunotherapy for Human Cancer. Science 2015, 348, 62–68. [PubMed: 25838374]

(16). Zhao C; Bai Z; Liu X; Zhang Y; Zou B; Zhong H Small GSH-Capped CuInS2 Quantum Dots: MPA-Assisted Aqueous Phase Transfer and Bioimaging Applications. ACS Appl. Mater. Inter. 2015, 7, 17623–17629.

(17). Syed AM; Sindhwani S; Wilhelm S; Kingston BR; Lee DSW; Gommerman JL; Chan WCW Three-Dimensional Imaging of Transparent Tissues via Metal Nanoparticle Labeling. J. Am. Chem. Soc 2017, 139, 9961–9971. [PubMed: 28641018]

(18). Fox CB; Cao Y; Nemeth CL; Chirra HD; Chevalier RW; Xu AM; Melosh NA; Desai TA Fabrication of Sealed Nanostraw Microdevices for Oral Drug Delivery. ACS Nano 2016, 10, 5873–5881. [PubMed: 27268699]

(19). Madrid M; Saklayen N; Shen W; Huber M; Vogel N; Mazur E Laser-Activated Self-Assembled Thermoplasmonic Nanocavity Substrates for Intracellular Delivery. ACS Appl. Bio. Mater 2018, 1, 1793–1799.

(20). Naldini L *Ex vivo* Gene Transfer and Correction for Cell-Based Therapies. Nat. Rev. Genet. 2011, 12, 301–315. [PubMed: 21445084]

(21). Cavazzana-Calvo M; Payen E; Negre O; Wang G; Hehir K; Fusil F; Down J; Denaro M; Brady T; Westerman K; Cavallesco R; Gillet-Legrand B; Caccavelli L; Sgarra R; Maouche-Chrétien L; Bernaudin F; Girot R; Dorazio R; Mulder G-J; Polack A; Bank A; Soulier J; Larghero J; Kabbara N; Dalle B; Gourmel B; Socie G; Chrétien S; Cartier N; Aubourg P; Fischer A; Cornetta K; Galacteros F; Beuzard Y; Gluckman E; Bushman F; Hacein-Bey-Abina S; Leboulch P Transfusion Independence and HMGA2 Activation after Gene Therapy of Human β-Thalassaemia. Nature 2010, 467, 318–322. [PubMed: 20844535]

(22). Stewart MP; Sharei A; Ding X; Sahay G; Langer R; Jensen KF *In Vitro* and *Ex vivo* Strategies for Intracellular Delivery. Nature 2016, 538, 183–192. [PubMed: 27734871]

(23). Stewart MP; Langer R; Jensen KF Intracellular Delivery by Membrane Disruption: Mechanisms, Strategies, and Concepts. Chem. Rev. 2018, 118, 7409–7531. [PubMed: 30052023]

(24). Belling JN; Heidenreich LK; Tian Z; Mendoza AM; Chiou TT; Gong Y; Chen NY; Young TD; Wattanatorn N; Park JH; Scarabelli L; Chiang N; Takahashi J; Young SG; Stieg AZ; De Oliveira S; Huang TJ; Weiss PS; Jonas SJ Acoustofluidic Sonoporation for Gene Delivery to Human Hematopoietic Stem and Progenitor Cells. Proc. Natl. Acad. Sci. U. S. A. 2020, 117, 10976–10982. [PubMed: 32358194]

(25). Thomas CE; Ehrhardt A; Kay MA Progress and Problems with the Use of Viral Vectors for Gene Therapy. Nat. Rev. Genet. 2003, 4, 346–358. [PubMed: 12728277]

(26). Kotterman MA; Chalberg TW; Schaffer DV Viral Vectors for Gene Therapy: Translational and Clinical Outlook. Annu. Rev. Biomed. Eng. 2015, 17, 63–89. [PubMed: 26643018]

(27). Qu Y; Zhang Y; Yu Q; Chen H Surface-Mediated Intracellular Delivery by Physical Membrane Disruption. ACS Appl. Mater. Inter. 2020, 12, 31054–31078.

(28). Tay A The Benefits of Going Small: Nanostructures for Mammalian Cell Transfection. ACS Nano 2020, Article ASAP.

(29). Sharei A; Zoldan J; Adamo A; Sim WY; Cho N; Jackson E; Mao S; Schneider S; Han M-J; Lytton-Jean A; Basto PA; Jhunjhunwala S; Lee J; Heller DA; Kang JW; Hartoularos GC; Kim K-S; Anderson DG; Langer R; Jensen KF A Vector-Free Microfluidic Platform for Intracellular Delivery. Proc. Natl. Acad. Sci. U. S. A. 2013, 110, 2082–2087. [PubMed: 23341631]

(30). Chiappini C; Campagnolo P; Almeida CS; Abbassi-Ghadi N; Chow LW; Hanna GB; Stevens MM Mapping Local Cytosolic Enzymatic Activity in Human Esophageal Mucosa with Porous Silicon Nanoneedles. Adv. Mater. 2015, 27, 5147–5152. [PubMed: 26197973]

(31). Seong H; Higgins SG; Penders J; Armstrong JPK; Crowder SW; Moore AC; Sero JE; Becce M; Stevens MM Size-Tunable Nanoneedle Arrays for Influencing Stem Cell Morphology, Gene Expression, and Nuclear Membrane Curvature. ACS Nano 2020, 14, 5371–5381. [PubMed: 32330008]

(32). Kang G; Carlson DW; Kang TH; Lee S; Haward SJ; Choi I; Shen AQ; Chung AJ Intracellular Nanomaterial Delivery *via* Spiral Hydroporation. ACS Nano 2020, 14, 3048–3058. [PubMed: 32069037]

(33). Tay A; Melosh N Nanostructured Materials for Intracellular Cargo Delivery. Acc. Chem. Res 2019, 52, 2462–2471. [PubMed: 31465200]

(34). Dixit HG; Starr R; Dundon ML; Pairs PI; Yang X; Zhang Y; Nampe D; Ballas CB; Tsutsui H; Forman SJ; Brown CE; Rao MP Massively-Parallelized, Deterministic Mechanoporation for Intracellular Delivery. Nano Lett. 2020, 20, 860–867. [PubMed: 31647675]

(35). Deng Y; Kizer M; Rada M; Sage J; Wang X; Cheon DJ; Chung AJ Intracellular Delivery of Nanomaterials *via* an Inertial Microfluidic Cell Hydroporator. Nano Lett. 2018, 18, 2705–2710. [PubMed: 29569926]

(36). Chopra A; Krishnan S; Simmel FC Electrotransfection of Polyamine Folded DNA Origami Structures. Nano Lett. 2016, 16, 6683–6690. [PubMed: 27608719]

(37). Geng T; Zhan YH; Wang J; Lu C Transfection of Cells Using Flow-through Electroporation Based on Constant Voltage. Nat. Protoc 2011, 6, 1192–1208. [PubMed: 21799488]

(38). Lukianova-Hleb EY; Mutonga MBG; Lapotko DO Cell-Specific Multifunctional Processing of Heterogeneous Cell Systems in a Single Laser Pulse Treatment. ACS Nano 2012, 6, 10973–10981. [PubMed: 23167546]

(39). Xiong RH; Raemdonck K; Peynshaert K; Lentacker I; De Cock I; Demeester J; De Smedt SC; Skirtach AG; Braeckmans K Comparison of Gold Nanoparticle Mediated Photoporation: Vapor Nanobubbles Outperform Direct Heating for Delivering Macromolecules in Live Cells. ACS Nano 2014, 8, 6288–6296. [PubMed: 24870061]

(40). Sengupta A; Kelly SC; Dwivedi N; Thadhani N; Prausnitz MR Efficient Intracellular Delivery of Molecules with High Cell Viability Using Nanosecond-Pulsed Laser-Activated Carbon Nanoparticles. ACS Nano 2014, 8, 2889–2899. [PubMed: 24547946]

(41). Kalies S; Heinemann D; Schomaker M; Gentemann L; Meyer H; Ripken T Immobilization of Gold Nanoparticles on Cell Culture Surfaces for Safe and Enhanced Gold Nanoparticle-Mediated Laser Transfection. J. Biomed. Opt. 2014, 19.

(42). Li M; Lohmuller T; Feldmann J Optical Injection of Gold Nanoparticles into Living Cells. Nano Lett. 2015, 15, 770–775. [PubMed: 25496343]

(43). Lukianova-Hleb E; Hu Y; Latterini L; Tarpani L; Lee S; Drezek RA; Hafner JH; Lapotko DO Plasmonic Nanobubbles as Transient Vapor Nanobubbles Generated around Plasmonic Nanoparticles. ACS Nano 2010, 4, 2109–2123. [PubMed: 20307085]

(44). Lyu ZL; Zhou F; Liu Q; Xue H; Yu Q; Chen H A Universal Platform for Macromolecular Delivery into Cells Using Gold Nanoparticle Layers *via* the Photoporation Effect. Adv. Funct. Mater. 2016, 26, 5787–5795.

(45). Tong S; Moyo B; Lee CM; Leong K; Bao G Engineered Materials for in vivo Delivery of Genome-Editing Machinery. Nat. Rev. Mater 2019, 4, 726–737. [PubMed: 34094589]

(46). Lee WG; Demirci U; Khademhosseini A Microscale Electroporation: Challenges and Perspectives for Clinical Applications. Integr. Biol 2009, 1, 242–251.

(47). Priceman SJ; Tilakawardane D; Jeang B; Aguilar B; Murad JP; Park AK; Chang WC; Ostberg JR; Neman J; Jandial R; Portnow J; Forman SJ; Brown CE Regional Delivery of Chimeric Antigen Receptor-Engineered T Cells Effectively Targets HER2(+) Breast Cancer Metastasis to the Brain. Clin. Cancer Res. 2018, 24, 95–105. [PubMed: 29061641]

(48). Shi J; Ma Y; Zhu J; Chen Y; Sun Y; Yao Y; Yang Z; Xie J A Review on Electroporation-Based Intracellular Delivery. Molecules 2018, 23, 3044.

(49). Stewart MP; Langer R; Jensen KF Intracellular Delivery by Membrane Disruption: Mechanisms, Strategies, and Concepts. Chem. Rev 2018, 118, 7409–7531. [PubMed: 30052023]

(50). Xu XB; Liu C; Kim K; Fan DL Electric-Driven Rotation of Silicon Nanowires and Silicon Nanowire Motors. Adv. Funct. Mater 2014, 24, 4843–4850.

(51). Kim W; Ng JK; Kunitake ME; Conklin BR; Yang P Interfacing Silicon Nanowires with Mammalian Cells. J. Am. Chem. Soc 2007, 129, 7228–7229. [PubMed: 17516647]

(52). Xie X; Xu AM; Leal-Ortiz S; Cao Y; Garner CC; Melosh NA Nanostraw–Electroporation System for Highly Efficient Intracellular Delivery and Transfection. ACS Nano 2013, 7, 4351–4358. [PubMed: 23597131]

(53). VanDersarl JJ; Xu AM; Melosh NA Nanostraws for Direct Fluidic Intracellular Access. Nano Lett. 2012, 12, 3881–3886. [PubMed: 22166016]

(54). He G; Feng J; Zhang A; Zhou L; Wen R; Wu J; Yang C; Yang J; Li C; Chen D; Wang J; Hu N; Xie X Multifunctional Branched Nanostraw-Electroporation Platform for Intracellular Regulation and Monitoring of Circulating Tumor Cells. Nano Lett. 2019, 19, 7201–7209. [PubMed: 31557044]

(55). Chiappini C; De Rosa E; Martinez JO; Liu X; Steele J; Stevens MM; Tasciotti E Biodegradable Silicon Nanoneedles Delivering Nucleic Acids Intracellularly Induce Localized *In vivo* neovascularization. Nat. Mater. 2015, 14, 532–539. [PubMed: 25822693]

(56). Peer E; Artzy-Schnirman A; Gepstein L; Sivan U Hollow Nanoneedle Array and Its Utilization for Repeated Administration of Biomolecules to the Same Cells. ACS Nano 2012, 6, 4940–4946. [PubMed: 22632128]

(57). Xie X; Xu AM; Angle MR; Tayebi N; Verma P; Melosh NA Mechanical Model of Vertical Nanowire Cell Penetration. Nano Lett. 2013, 13, 6002–6008. [PubMed: 24237230]

(58). Wang Y; Yang Y; Yan L; Kwok SY; Li W; Wang Z; Zhu X; Zhu G; Zhang W; Chen X; Shi P Poking Cells for Efficient Vector-Free Intracellular Delivery. Nat. Commun 2014, 5, 4466. [PubMed: 25072981]

(59). Lee SE; Sasaki DY; Park Y; Xu R; Brennan JS; Bissell MJ; Lee LP Photonic Gene Circuits by Optically Addressable siRNA-Au Nanoantennas. ACS Nano 2012, 6, 7770–7780. [PubMed: 22827439]

(60). Xin H; Namgung B; Lee LP Nanoplasmonic Optical Antennas For life Sciences and Medicine. Nat. Rev. Mater 2018, 3, 228–243.

(61). Boulais E; Lachaine R; Meunier M Plasma Mediated Off-Resonance Plasmonic Enhanced Ultrafast Laser-Induced Nanocavitation. Nano Lett. 2012, 12, 4763–4769. [PubMed: 22845691]

(62). Furlani EP; Karampelas IH; Xie Q Analysis of Pulsed Laser Plasmon-Assisted Photothermal Heating and Bubble Generation at the Nanoscale. Lab Chip 2012, 12, 3707–3719. [PubMed: 22782691]

(63). Prentice P; Cuschieri A; Dholakia K; Prausnitz M; Campbell P Membrane Disruption by Optically Controlled Microbubble Cavitation. Nat. Phys. 2005, 1, 107–110.

(64). Wu TH; Teslaa T; Kalim S; French CT; Moghadam S; Wall R; Miller JF; Witte ON; Teitell MA; Chiou PY Photothermal Nanoblade for Large Cargo Delivery into Mammalian Cells. Anal. Chem 2011, 83, 1321–1327. [PubMed: 21247066]

(65). Ghosh P; Han G; De M; Kim CK; Rotello VM Gold Nanoparticles in Delivery Applications. Adv. Drug. Deliver. Rev 2008, 60, 1307–1315.

(66). Peng T; Li X; Li K; Nie Z; Tan W DNA-Modulated Plasmon Resonance: Methods and Optical Applications. ACS Appl. Mater. Inter 2020, 12, 14741–14760.

(67). Pitsillides CM; Joe EK; Wei X; Anderson RR; Lin CP Selective Cell Targeting with Light-Absorbing Microparticles and Nanoparticles. Biophys. J 2003, 84, 4023–4032. [PubMed: 12770906]

(68). Man T; Zhu X; Chow YT; Dawson ER; Wen X; Patananan AN; Liu TL; Zhao C; Wu C; Hong JS; Chung PS; Clemens DL; Lee BY; Weiss PS; Teitell MA; Chiou PY Intracellular Photothermal Delivery for Suspension Cells Using Sharp Nanoscale Tips in Microwells. ACS Nano 2019, 13, 10835–10844. [PubMed: 31487464]

(69). Odom TW; Love JC; Wolfe DB; Paul KE; Whitesides GM Improved Pattern Transfer in Soft Lithography Using Composite Stamps. Langmuir 2002, 18, 5314–5320.

(70). Qin D; Xia Y; Whitesides GM Soft Lithography for Micro- and Nanoscale Patterning. Nat. Protocols 2010, 5, 491–502. [PubMed: 20203666]

(71). Kumar A; Whitesides GM Features of Gold Having Micrometer to Centimeter Dimensions Can Be Formed through a Combination of Stamping with an Elastomeric Stamp and an Alkanethiol “Ink” Followed by Chemical Etching. Appl. Phys. Lett 1993, 63, 2002–2004.

(72). Andrews AM; Liao WS; Weiss PS Double-Sided Opportunities Using Chemical Lift-Off Lithography. Acc. Chem. Res 2016, 49, 1449–1457. [PubMed: 27064348]

(73). Cao HH; Nakatsuka N; Serino AC; Liao W-S; Cheunkar S; Yang H; Weiss PS; Andrews AM Controlled DNA Patterning by Chemical Lift-Off Lithography: Matrix Matters. ACS Nano 2015, 9, 11439–11454. [PubMed: 26426585]

(74). Kim J; Rim YS; Chen H; Cao HH; Nakatsuka N; Hinton HL; Zhao C; Andrews AM; Yang Y; Weiss PS Fabrication of High-Performance Ultrathin In2O3 Film Field-Effect Transistors and Biosensors Using Chemical Lift-Off Lithography. ACS Nano 2015, 9, 4572–4582. [PubMed: 25798751]

(75). Srinivasan C; Mullen TJ; Hohman JN; Anderson ME; Dameron AA; Andrews AM; Dickey EC; Horn MW; Weiss PS Scanning Electron Microscopy of Nanoscale Chemical Patterns. ACS Nano 2007, 1, 191–201. [PubMed: 19206649]

(76). Smith RK; Lewis PA; Weiss PS Patterning Self-Assembled Monolayers. Prog. Surf. Sci 2004, 75, 1–68.

(77). Liao W-S; Cheunkar S; Cao HH; Bednar HR; Weiss PS; Andrews AM Subtractive Patterning *via* Chemical Lift-Off Lithography. Science 2012, 337, 1517–1521. [PubMed: 22997333]

(78). Vaish A; Shuster MJ; Cheunkar S; Weiss PS; Andrews AM Tuning Stamp Surface Energy for Soft Lithography of Polar Molecules to Fabricate Bioactive Small-Molecule Microarrays. Small 2011, 7, 1471–1479. [PubMed: 21538866]

(79). Zhao C; Xu X; Bae SH; Yang Q; Liu W; Belling JN; Cheung KM; Rim YS; Yang Y; Andrews AM; Weiss PS Large-Area, Ultrathin Metal-Oxide Semiconductor Nanoribbon Arrays Fabricated by Chemical Lift-Off Lithography. Nano Lett. 2018, 18, 5590–5595. [PubMed: 30060654]

(80). Zhao C; Xu X; Yang Q; Man T; Jonas SJ; Schwartz JJ; Andrews AM; Weiss PS Self-Collapse Lithography. Nano Lett. 2017, 17, 5035–5042. [PubMed: 28737930]

(81). Zhao C; Xu X; Chiang N; Yang Q; Liu W; Schwartz JJ; Andrews AM; Weiss PS Two-Dimensional Plasmonic Nanostructure Arrays Fabricated by Double-Patterning Chemical Lift-Off Lithography. 2020, In prep.

(82). Carlson A; Bowen AM; Huang Y; Nuzzo RG; Rogers JA Transfer Printing Techniques for Materials Assembly and Micro/Nanodevice Fabrication. Adv. Mater 2012, 24, 5284–5318. [PubMed: 22936418]

(83). Raun A; Saklayen N; Zgrabik C; Shen W; Madrid M; Huber M; Hu E; Mazur E A Comparison of Inverted and Upright Laser-Activated Titanium Nitride Micropyramids for Intracellular Delivery. Sci. Rep 2018, 8, 15595. [PubMed: 30349063]

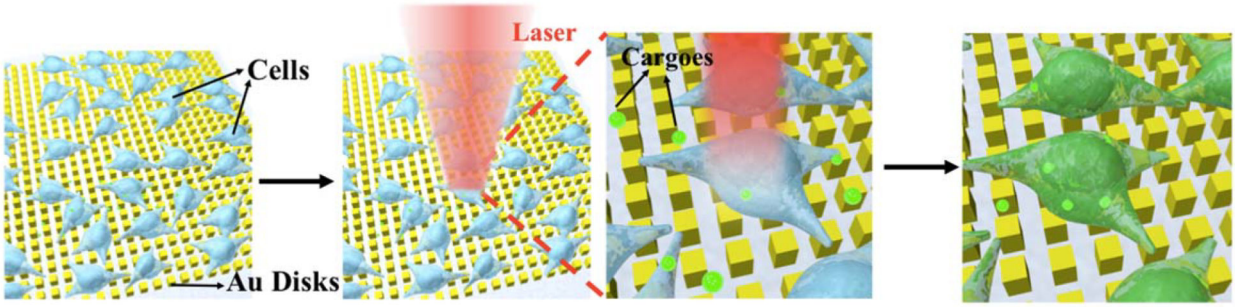

Figure 1.

Illustration of photothermal intracellular delivery enabled by localized surface plasmon resonance (LSPR) of gold nanodisks excited by a nanosecond laser. After cell seeding, the laser was rastered over cells seeded onto the nanostructures and cultured in a medium containing membrane impermeable biomolecules. Upon irradiation, the gold plasmonic structures heat up rapidly and generate cavitation bubbles, which facilitate the delivery of the biomolecular cargo into targeted cells by creating transient pores along nearby their outer membranes.

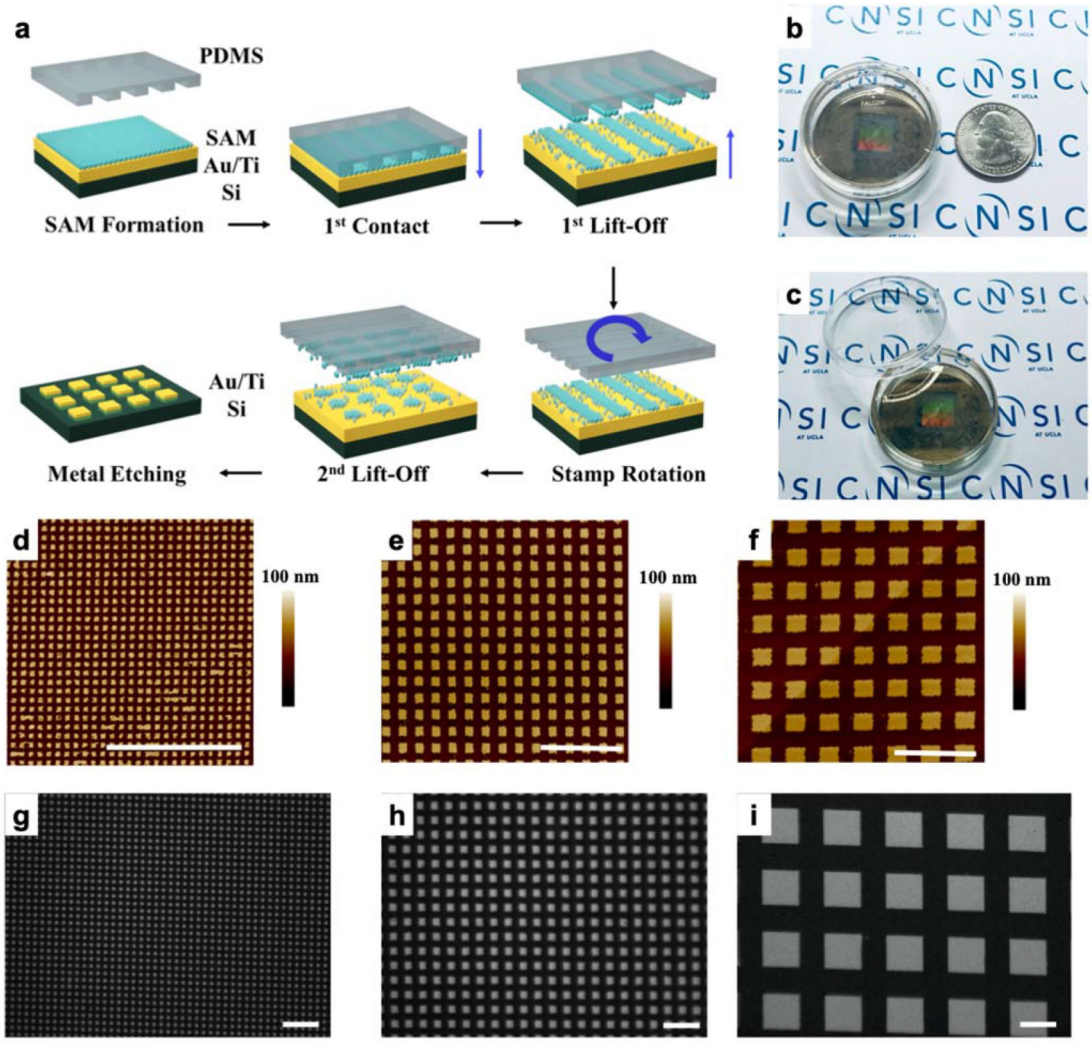

Figure 2.

Gold plasmonic disk arrays fabricated by double-patterning chemical lift-off lithography (CLL). (a) Schematic of the patterning process. Substrates were coated with gold (Au) before being functionalized with self-assembled monolayers (SAMs). Polydimethylsiloxane (PDMS) stamps with line patterns were “activated” by exposure to an oxygen plasma to generate hydrophilic silanol groups on their surfaces. The stamps were then placed in conformal contact with the substrate. Molecules were selectively removed in the contact region upon lifting the stamp. A second patterning step was then performed by rotating the stamp 90° to generate two dimensional (2D) nanosquare chemical patterns. Exposed metal was removed *via* wet etching to generate Au 2D nanodisk arrays. (b,c) Representative images of large-area 350-nm-wide Au nanodisk arrays on a plastic petri dish. (d-f) Atomic force microscope images of Au nanodisk arrays comprised of (d) 350-nm wide, (e) 1-μm wide, and (f) 2-μm wide features. (g-i) Optical microscope images of gold nanodisk arrays with feature widths (g) 1 μm, (h) 2 μm, and (i) 10 μm. Scale bars: 10 μm. CNSI at UCLA logo used with permission.

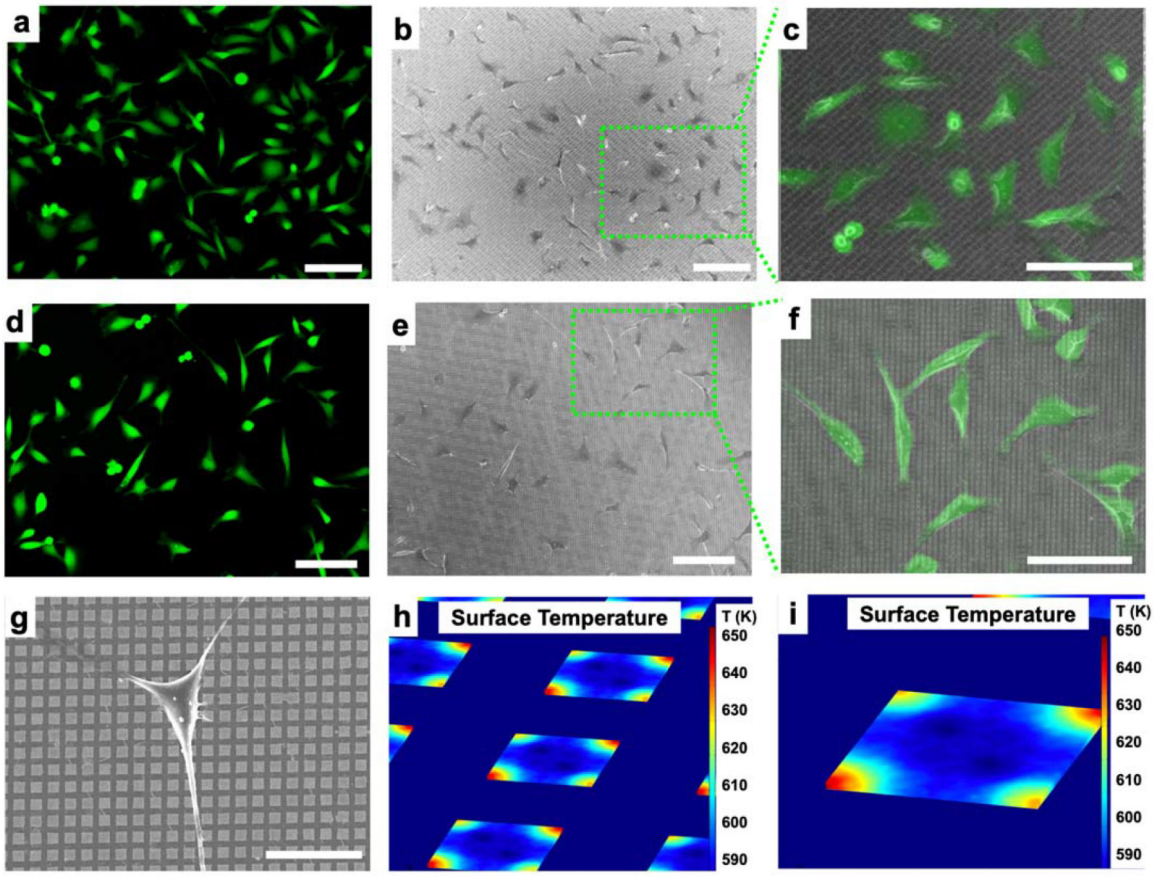

Figure 3.

(a) Fluorescence microscope images of HeLa cells on 1-μm-wide gold (Au) nanodisk arrays labeled with a cell membrane-impermeable dye (Calcein AM). (b) Scanning electron microscope images of fixed cells on a substrate. (c) Overlay of the green-box-designated region seen in (b) with (a). (d) Fluorescence microscope images of HeLa cells on 2-μm-wide gold (Au) nanodisk arrays labeled with a cell membrane impermeable dye (Calcein AM). (e) Scanning electron microscope images of fixed cells on a substrate. (f) Overlay of the green box-designated region seen in (b) with (a). (g) Scanning electron microscope image of single Hela cell on 2-μm-wide Au nanodisk array substrate. (h,i) Simulation results of surface temperature at the gold nanodisk array (1-μm wide) interface in water. Scale bars: (a-f) 100 μm, (g) 20 μm.

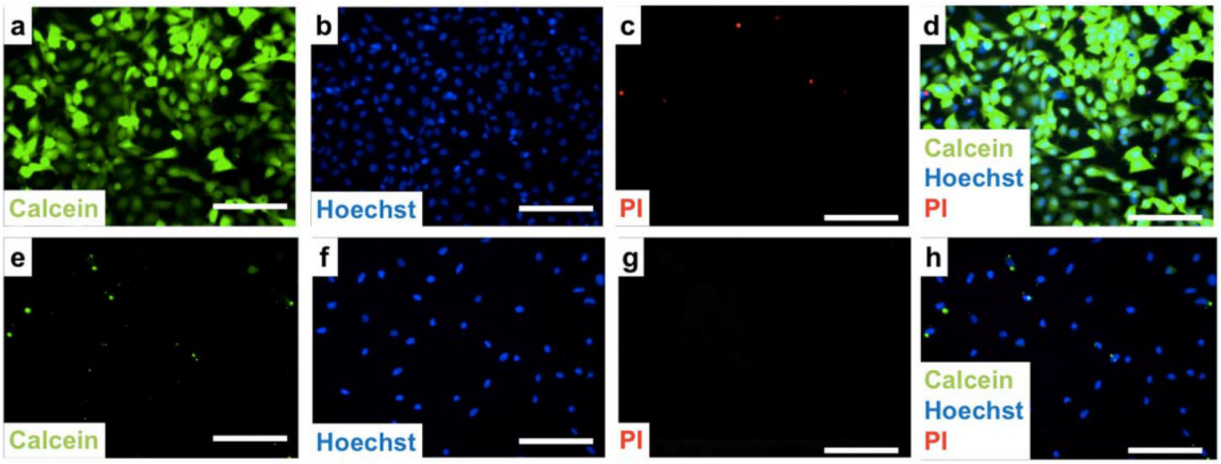

Figure 4.

Delivery efficiency and cell viability testing. (a-d) Delivery of calcein to HeLa cells using gold nanodisk arrays (1 μm wide, 2 μm pitch, 30 nm thickness) under laser irradiation with 11 mJ/cm^2 fluence. (a) Representative image of delivery of calcein (green) to targeted cells. (b) Cell nuclei are stained with Hoechst 33342 to label both live and dead cells (blue). (c) Propidium iodide (PI) assay to identify dead cells (red). (d) Overlaid image of calcein, Hoechst 33342, and PI dyes. Efficiency was found to be 98 ± 1%, and viability is 99 ± 1%. (e–h) Control experiment using flat gold thin film under the same laser irradiation of 11 mJ/cm^2 fluence, where (e) corresponds to the calcein channel, (f) is the Hoechst dye, (g) is the PI dye, and (h) is the overlaid image of (e–g). Scale bars: 100 μm.

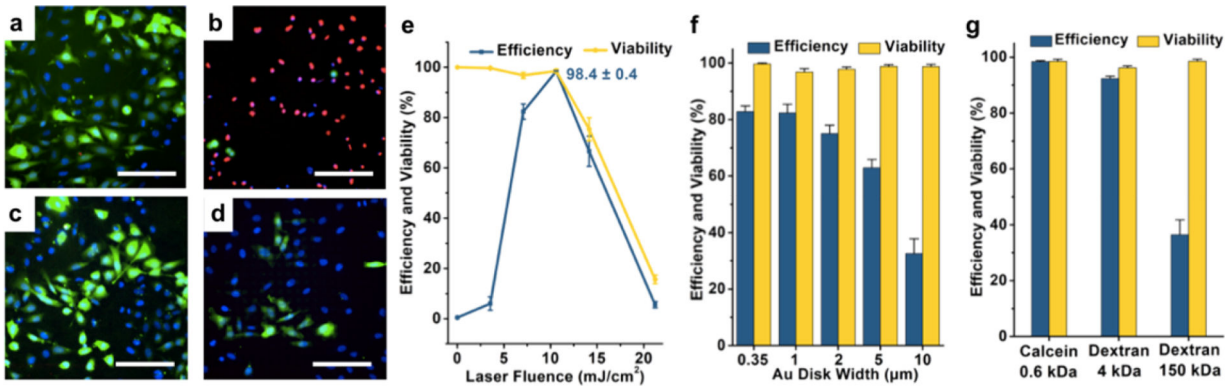

Figure 5.

Delivery efficiency and cell viability at different laser fluences and gold disk sizes are shown in overlaid images (a-d) of 0.6 kDa calcein delivery (green), Hoechst dye (blue), and PI dye (red). Delivery results under different laser fluence at (a) 7 mJ/cm^2, and (b) 21.2 mJ/cm^2, respectively, both on 1-μm wide nanodisk arrays. Delivery results using different sizes of gold nanodisk arrays of (c) 2 μm and (d) 10 μm widths, respectively, both under laser fluence of 7 mJ/cm^2. (e) Delivery efficiencies and viabilities after 90 min as a function of laser fluence on 1-μm wide nanodisk arrays. Error bars represented standard error mean (s.e.m.) (n = ~2,500 cells for all tests). (f) Delivery efficiencies and viabilities with different sizes of gold nanodisk arrays at 7 mJ/cm^2. Error bars, s.e.m. (n = ~1,900 cells for all tests). (g) Delivery efficiencies and viabilities with different cargoes at 11 mJ/cm^2 on 1-μm wide nanodisk arrays. Error bars, s.e.m. (n = ~2,000 cells for all tests). Scale bars: 100 μm.